

Article

Early Detection of Cavitation in Centrifugal Pumps Using Low-Cost Vibration and Sound Sensors

Marios Karagiovanidis ¹, Xanthoula Eirini Pantazi ^{1,*} , Dimitrios Papamichail ²  and Vassilios Fragos ¹ 

¹ Laboratory of Agricultural Engineering, Faculty of Agriculture, Aristotle University of Thessaloniki, 54124 Thessaloniki, Greece; mkaragiovanidis@gmail.com (M.K.); fragos@agro.auth.gr (V.F.)

² Laboratory of General & Agricultural Hydraulics & Land Reclamation, Faculty of Agriculture, Aristotle University of Thessaloniki, 54124 Thessaloniki, Greece; papamich@agro.auth.gr

* Correspondence: xpantazi@agro.auth.gr; Tel.: +30-2310991764

Abstract: The scope of this study is the evaluation of early detection methods for cavitation phenomena in centrifugal irrigation pumps by analyzing the produced vibration and sound signals from a low-cost sensor and data acquisition system and comparing several computational methods. Vibration data was acquired using the embedded accelerometer sensor of a smartphone device. Sound signals were obtained using the embedded microphone of the same commercial smartphone. The analysis was based on comparing the signals in different operating conditions with reference to the best efficiency operating point of the pump. In the case of vibrations, data was acquired for all three directional axes. The signals were processed by computational methods to extract the relative features in the frequency domain and use them to train an artificial neural network to be able to identify the different pump operating conditions while the cavitation phenomenon evolves. Three different classification algorithms were used to examine the most preferable approach for classifying data, namely the Classification Tree, the K-Nearest Neighbor, and the Support Vector Data algorithms. In addition, a convolutional neural network was utilized to examine the success rate of the classification when the datasets were formed as spectrograms instead. A detailed comparison of the classification algorithms and different axes was conducted. Comparing the results of the different methods for vibration and sound datasets, classification accuracy showed that in the case of vibration, the detection of cavitation in real conditions is possible, while it proves more challenging to identify cavitation conditions using sound data obtained with low-cost commercial sensors.

Keywords: centrifugal pump; cavitation; accelerometer; artificial neural network; predictive maintenance; signal analysis



Citation: Karagiovanidis, M.; Pantazi, X.E.; Papamichail, D.; Fragos, V. Early Detection of Cavitation in Centrifugal Pumps Using Low-Cost Vibration and Sound Sensors. *Agriculture* **2023**, *13*, 1544. <https://doi.org/10.3390/agriculture13081544>

Academic Editor: Gerard Arbat

Received: 24 May 2023

Revised: 23 July 2023

Accepted: 29 July 2023

Published: 2 August 2023



Copyright: © 2023 by the authors. Licensee MDPI, Basel, Switzerland. This article is an open access article distributed under the terms and conditions of the Creative Commons Attribution (CC BY) license (<https://creativecommons.org/licenses/by/4.0/>).

1. Introduction

Modern irrigation systems heavily rely on irrigation pumps, which are crucial for the expansion of irrigated areas. According to a study conducted by the Food and Agriculture Organization (FAO), developing countries are projected to increase their irrigated areas by 2420 square kilometers by 2030 [1]. As the demand for efficient irrigation systems grows, so do maintenance needs for irrigation pumps; hence, addressing common operational faults such as cavitation is becoming imperative.

Cavitation in water pumps occurs when the Available Net Positive Suction Head falls below the Required Net Positive Suction Head, causing the absolute static pressure within the pump to drop below the saturated vapor pressure of water at the given temperature. This leads to the formation of air bubbles, which subsequently collapse to generate high-pressure mini-hammer blows [2]. Cavitation can result in several undesirable effects, including a deterioration in the hydraulic performance of the pump, material erosion near the collapsing bubbles, vibration of the pump walls, and associated damage [2,3].

To prevent and rectify cavitation in irrigation centrifugal water pumps, early detection of the phenomenon is crucial. Various methods exist for monitoring pump operating conditions, either during operation or by inspecting the pump's interior. However, traditional reactive maintenance and invasive techniques have significant drawbacks compared to non-invasive alternatives. Shifting to proactive maintenance requires comprehensive research due to the need for process digitalization, scheduling, and an organized approach to maintenance [4]. Non-invasive methods, such as acoustic emissions, vibration analysis, and sensor-less detection utilizing deviations in motor electrical signals, are gaining popularity as they minimize system downtime and associated costs [5].

Over the past few decades, plenty of non-invasive maintenance techniques have been studied, some in greater detail and extent than others [6]. Adefemi et al. have developed a digital twin of a centrifugal pump to accurately predict its operating state given a predefined set of parameters [7]. Flow visualization through close-up imaging of cavitation formation is another tool for macroscopic identification studied extensively by Mousmoulis et al. [8]. This study directly links the impeller geometry with the cavitation magnitude, providing insights for the better design and assembly of irrigation pumps. Computational methods such as computational fluid dynamics (CFD) have been proven by Chen et al. to be effective in analyzing vibration and sound data for various types of compressors, including pumps and fans [9]. Artificial Neural Networks (ANN) and Convolutional Neural Networks (CNN) have been extensively developed for signal and image analysis, respectively, showing significant success in detecting operating conditions on different pump types [10,11].

Among the available data sources for pump condition monitoring and cavitation detection, sound and vibration data have received the most analysis [12]. Statistical analysis of acoustic data in the time and frequency domains provides valuable information for the relationship between the suction valve opening and cavitation formation. This relationship has been studied for both industrial and lab-scale setups by Neill et al. [13]. Al Obaidi has identified three distinct regions where changes in emitted pump sound vary from no change to significant change, depending on alteration in the suction valve opening [14]. A study by Leighton et al. has proven that acoustic data not only aids in cavitation detection and pump condition monitoring but also allows for estimations of cavitation scale and bubble population within a liquid [15]. Finally, deep learning techniques, including novel and improved CNN models, have demonstrated enhanced reliability in diagnosing deviations in pump operation [16] and piping leakage [17] using acoustic data

The direct correlation between vibration and the pump's operating state has also been extensively observed and studied, providing a foundation for further research in state detection and classification [18]. Ling et al. have proven that the combination of Internet of Things (IoT) technology and advanced machine learning methods offers cost-effective and user-friendly tools for condition monitoring in irrigation pump operation with high reliability [19]. Previous studies have also explored the use of artificial intelligence (AI) in preventive maintenance, utilizing techniques such as support vector machine (SVM) algorithms for vibration-based pump failure detection [20,21]. Other methods, including the K-Nearest Neighbor (KNN) and the Classification Tree algorithms, have been employed for diagnosing faulty operations in microgrids [21].

In this study, both acoustic and vibration data are obtained from a centrifugal pump using a smartphone device in order to evaluate which is the best signal to use. Acoustic data can be obtained using any type of microphone in close proximity to the pump. Vibration data can be acquired through either contact measurement, involving instrumentation like accelerometers attached to the vibration source, or non-contact measurement, which employs electromagnetic radiation from data transmission [22].

Detecting the cavitation phenomenon and determining its occurrence window in centrifugal pumps is crucial for both preventive maintenance and the optimal design of mechanical components such as blades. Kyparissis and Margaritis have investigated the effects of design parameters on cavitation formation and the overall performance

of centrifugal pumps, emphasizing the importance of understanding where and how cavitation occurs in different pump designs [16,23].

Previous studies focusing on the detection and monitoring of cavitation in irrigation pumps were based on lab setups and sophisticated data acquisition systems with industrial vibration or acoustic emission sensors or even high-tech cameras [13,16,23].

A summary of the main methods for detecting cavitation in centrifugal pumps is provided in Table 1 below.

Table 1. Summary of methods used for detecting cavitation in centrifugal pumps.

Detection Method	Description	Literature
Digital Twins and simulation models	Accurately predict the operating state of a centrifugal pump through simulation models	[4,7]
Sensor-less Detection	Utilizing deviations in motor electrical signals to detect cavitation	[5]
Vibration Analysis	Monitoring vibrations caused by cavitation-induced instabilities	[18–22]
Acoustic Emission Analysis	Detecting acoustic signals generated during cavitation events	[13–17]
Flow Visualization	Close-up imaging of cavitation formation to study impeller geometry and cavitation magnitude	[8]
Computation Fluid Dynamics (CFD)	Analyzing vibration and sound data for various types of compressors, including pumps and fans	[9]
Artificial Neural Networks (ANN)	Utilizing neural networks for signal and image analysis to detect operating conditions	[10,19–21]
Convolutional Neural Networks (CNN)	Employing CNN models for diagnosing deviations in pump operation and piping leakage using acoustic data	[11,16,17]

The scope of this study was to assess and compare four standard classification methods using raw signals from a low-cost data acquisition platform, ultimately identifying a simple yet highly reliable algorithm for detecting cavitation. By using signal and vibration data with minimum processing (no feature extraction) and leveraging machine learning and deep learning techniques, the research explored their effectiveness in fault detection and condition monitoring of centrifugal pumps, providing invaluable insights for future advancements in IoT-integrated real-time fault detection and operation monitoring applications. What sets this research apart is the emphasis given to simulating a real-life irrigation system and utilizing a low-cost device that simultaneously acquires sound and vibration data, commonly owned by farmers and operators. Combining those data with a well-trusted, robust algorithm, real-time early detection can be achieved, and preventive maintenance and proactive control of centrifugal pumps are possible.

Measurements were conducted on the experimental setup, consisting of a water tank, a single-stage centrifugal pump, pressure sensors and transmitters, a flow meter, and hydraulic piping with control valves and gauges. Vibration data was acquired using the smartphone's embedded axial accelerometer and recording software, while sound signals were captured using the smartphone's built-in microphone.

The experiment compared the obtained signals under different operating conditions, referencing the manufacturer's operating curve and theoretical calculations for the pump's optimal efficiency. Subsequently, the experimental results were analyzed, focusing on the accuracy of the classification methods used and the correlation of vibration data along each axis with the evolving cavitation phenomenon. The classification methods for vibration signals achieved an overall success rate of over 90%, with the KNN and SVM methods achieving 100% success for data sets in the flow direction, CNN achieving nearly 97% success, and the Classification Tree method achieving approximately 90% success. In contrast, the classification methods for sound signals achieved only a 30% success rate, with the SVM method reaching a maximum of 54% success, indicating that sound data is less reliable than vibration data and more susceptible to factors like ambient noise.

2. Materials and Methods

2.1. Experimental Setup

The experimental setup involved utilizing a complete water pumping station configuration. To replicate a range of operating conditions, throttling valves were incorporated into both the suction and discharge lines. Additionally, a flow sensor was installed in the discharge line to measure the water flow rate. To monitor the pressure levels, sensors were placed in both the suction and discharge lines. Figure 1 provides a visual representation of the experimental setup in the form of a simple piping and instrumentation diagram (P&ID), while Table 2 presents a detailed list of the components comprising the setup. These components collectively form an integral part of the experimental apparatus.

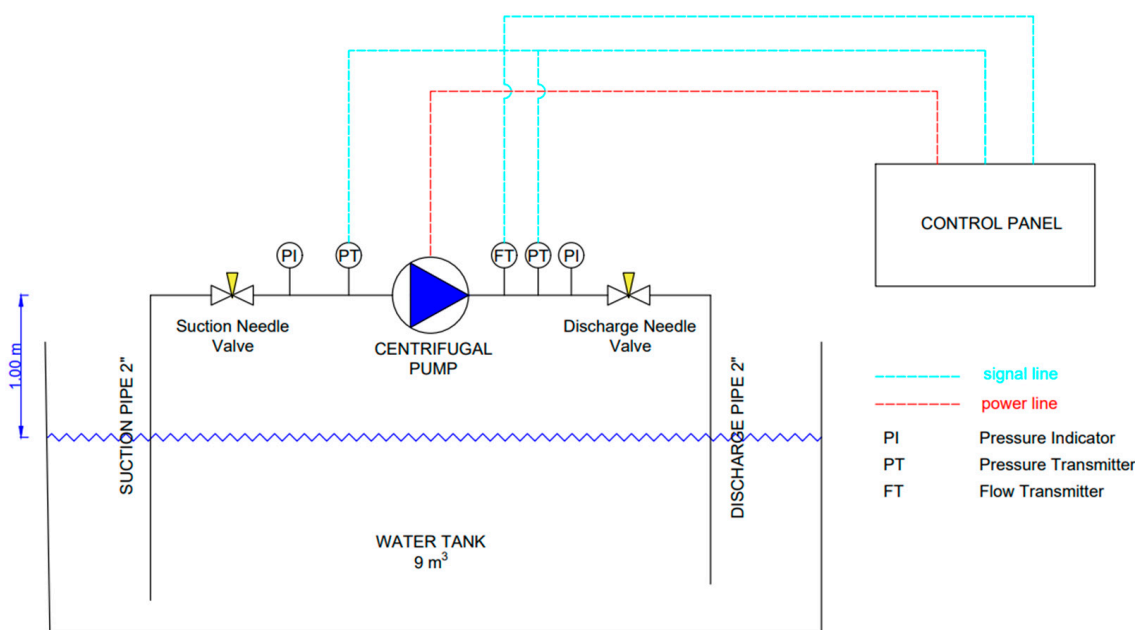


Figure 1. Experimental Setup Piping and Instrumentation Diagram.

Table 2. Main equipment characteristics.

Instrument	Characteristics
Pump	SAER, IR 40–160 NB/B, centrifugal, closed impeller, single stage
Motor	SAER, 400 V, 4 kW, 2900 rpm
Flowmeter	DANFOSS, MagFlow MAG 3100, Electromagnetic
Discharge line pressure sensor	WICA, ECO-1, 0–48 bar
Suction line pressure sensor	Delta, DPA01M, –1 to 1 bar
Suction piping	Steel, DN50, non-return valve, throttling valve
Discharge piping	Steel, DN50, throttling valve
Water tank	Steel, volume 9 m ³

The pump that was used for the experimental setup is shown in Figure 2. The data acquisition platform employed for the experiment was a Samsung Galaxy A52s 5G smartphone, securely attached to the pump’s casing using a rigid metal plate, as depicted in Figure 3. To capture acceleration data, the smartphone’s embedded acceleration sensor (ICM42605M Accelerometer -TDK InvenSense, resolution: 0.002394 m/s², maximum range: 78.453201 m/s²). The sampling frequency was set to the maximum available range of 500–510 Hz. The recorded acceleration data was stored in a .txt file format using the smartphone’s onboard SD card.

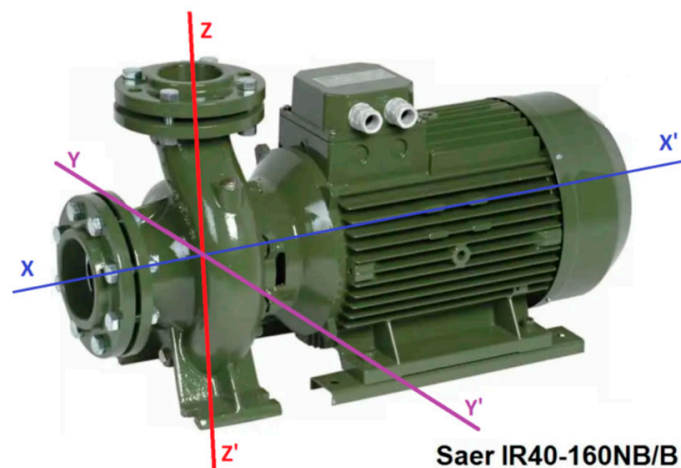


Figure 2. Pump and corresponding 3D axis system (courtesy of SAER Elettropompe Spa).



Figure 3. Actual mounting of the smart phone on the pump casing, using a rigid metal plate.

For capturing sound data, the smartphone's embedded microphone was employed. Although the microphone is primarily designed for capturing ambient sounds in videos and stereo sound recordings, it was utilized in this experiment. The microphone had a frequency response range, and a sampling frequency of 44.1 kHz was selected. The sensitivity of the microphone was -42 dBFS.

During the experiment, the ambient temperature was measured to be 15.7 °C, while the water temperature remained constant at 11 °C. The voltage supplied to the pump motor varied between 231 V and 235 V for each phase. The pump's rotational speed was maintained at a constant 2900 rpm, which corresponds to the nominal electric motor speed at a 50 Hz frequency of AC current.

2.2. Data Collection Methodology

Starting the experiment, the pump was run at the Best Efficiency Point (BEP), based on the manufacturer's performance curves (Figure 4), to acquire reference state data and for enough time to equalize water temperature in the pump body.

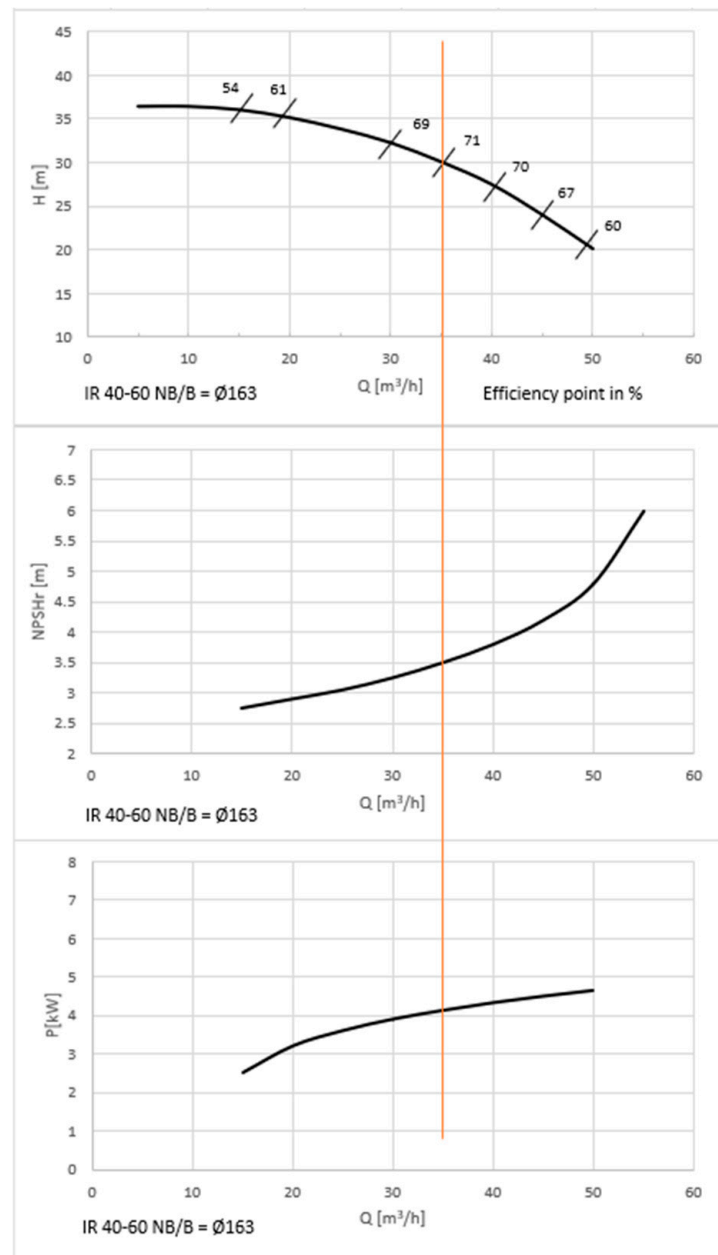


Figure 4. SAER IR 40–160 NB/B Performance curves based on water’s kinematic viscosity of $1 \text{ mm}^2/\text{s}$, density of $1000 \text{ kg}/\text{m}^3$, and temperature of $15 \text{ }^\circ\text{C}$. Tolerance and curves according to UNI EN ISO 9906.

To ensure consistent data collection and stabilize the water temperature within the pump body, the experiment began by operating the pump at the Best Efficiency Point (BEP), as indicated by the manufacturer’s performance curves, shown in orange in Figure 5.

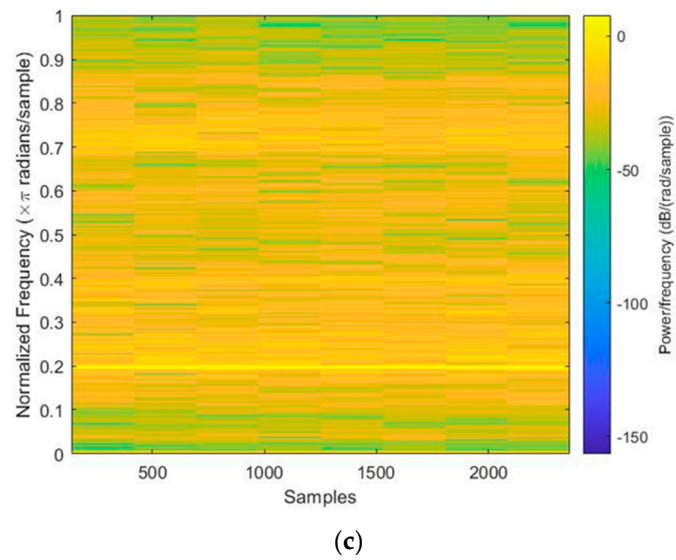
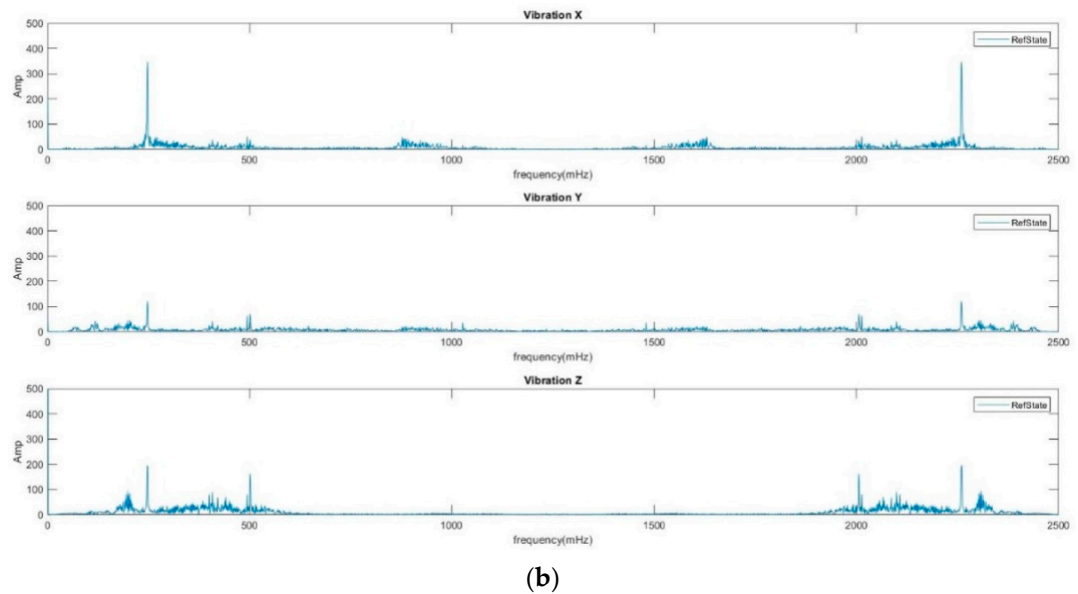
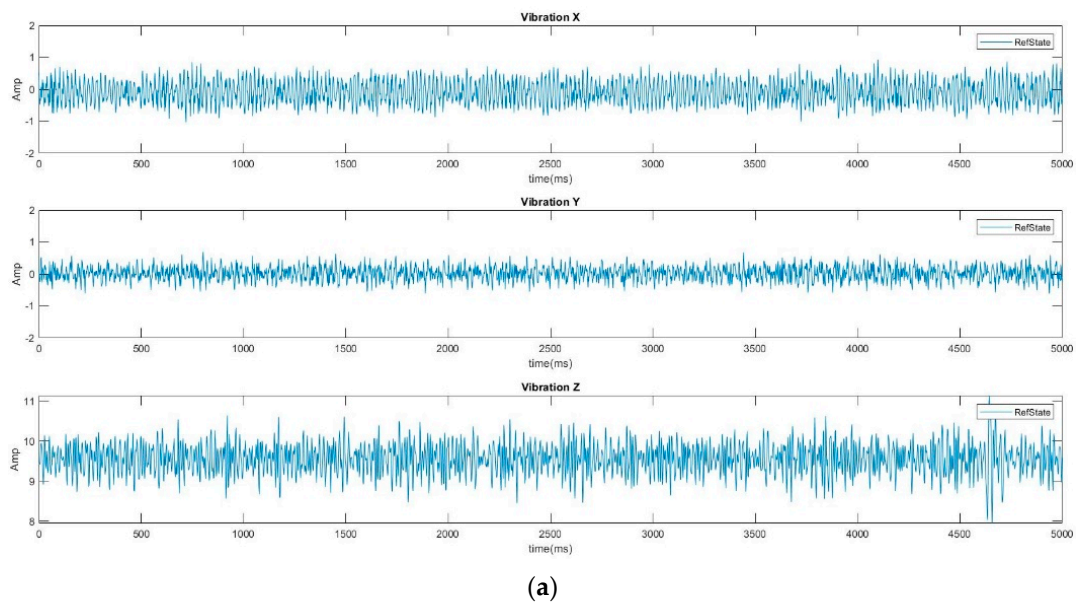


Figure 5. Cont.

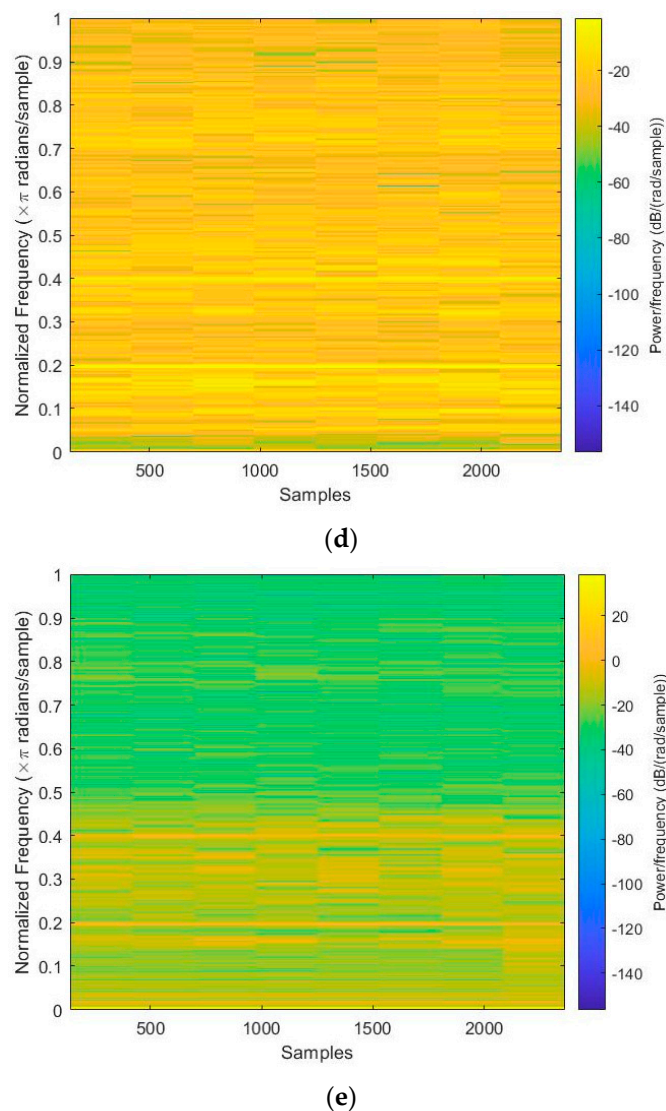


Figure 5. Indicative vibration data plots for State 2, as exported by MATLAB[®] 6.5 (R13), (a) time domain—msec vs. amplitude; (b) frequency domain—mHz vs. amplitude; (c–e) spectrogram for x , y , and z axes (normalized frequency ($\times \pi$ radians/sample) and power/frequency (dB/rad/sample)).

By throttling (opening or choking) the suction or discharge valve progressively, ten different operating conditions for ten different states were achieved.

State 0 corresponds to a fully closed discharge valve and a fully open suction valve, where there is no flow and the vibration and sound of the pump are minimal. Cavitation is not present in this state, but since water pumps are cooled down by the water flow, operating with no flow will eventually lead to overheating and damage to the bearings, the sealing elements, and the main components, such as the impeller and casing. State 1 corresponds to the normal operating conditions of the pump as close as possible to the best efficiency point of the pump, given the fact that the minimum existing suction height, the piping system, the valves, and the instrumentation affect the total performance. In this state, the suction valve is fully open, and the discharge valve is gradually opened to achieve the pressure and flow indicated by the manufacturer at the best efficiency point. States 2, 3, and 4 correspond to an increasingly choked suction valve and the gradual development of the suction cavitation phenomenon. By choking the suction valve, water velocity is increased, and cavitation conditions are evolving in the pump casing and around the impeller. Increased water velocity and cavitation lead to increased vibration of the pump and noise changes. State 5 corresponds to a fully closed suction valve where output

pressure and flow are zero and the suction head is maximum. In this state, there is no cavitation, but exactly as in state 0, eventually the pump components will overheat and cause severe damage. The vibration and sound of the pump are again of low magnitude, as in state 0. For States 6, 7, and 8, the suction valve is fully open, but the discharge valve is now gradually opened, leading to higher flow and lower discharge pressure, thus leaving the best efficiency operating point. Finally, State 9 corresponds to a fully open discharge valve where the water velocity is at its highest point and the discharge cavitation phenomenon is fully evolved. In this state, the pump contains a great deal of gas bubbles, and vibration starts to decrease because of the absorption of pressure energy by the bubbles themselves. At the same time, bubbles absorb pump energy, and delivery heads drop rapidly [24]. The operational states at which the pump was tested are coded in Table 3.

Table 3. Experimental setup characteristics, State 1 highlighted to indicate nominal state.

State ID	Description
State 0	Operation with a fully closed discharge valve (zero flow)
State 1	Operation at optimal conditions (best efficiency point)
State 2	Operation with choked suction valve (step 1—20%)
State 3	Operation with choked suction valve (step 2—40%)
State 4	Operation with choked suction valve (step 3—60%)
State 5	Operation with a fully closed suction valve (step 4—zero flow)
State 6	Over-pumping operation (step 1)
State 7	Over-pumping operation (step 2)
State 8	Over-pumping operation (step 3)
State 9	Over-pumping operation (step 4—fully open discharge valve)

Auxiliary data was recorded for each state to define the operating state of the pump compared to the manufacturer’s running curves and as opposed to the “Best Efficiency Operating State (State 1) and are presented in Table 4”. Recorded auxiliary data are:

1. Discharge Flowrate (2 m after pump casing): Q_{out}
2. Discharge Pressure (1 m after pump casing): P_{out}
3. Suction Pressure (0.5 m before pump casing): P_{in}
4. Current of each phase: I_1, I_2, I_3

Table 4. Auxiliary measured values for each operational state.

State ID	Q_{out} (m ³ /h)	P_{in} (Bar)	P_{out} (Bar)	I_1 (A)	I_2 (A)	I_3 (A)
State 0	00.13	−0.10	3.60	4.98	5.41	5.50
State 1	28.92	−0.32	3.00	7.26	7.68	7.88
State 2	27.70	−0.60	2.70	7.04	7.57	7.66
State 3	26.80	−0.80	2.50	6.82	7.36	7.44
State 4	18.80	−0.90	1.00	5.52	6.06	6.04
State 5	01.66	−0.92	0.00	4.98	5.52	5.50
State 6	36.20	−0.46	2.50	7.91	8.44	8.52
State 7	42.00	−0.59	2.00	8.45	8.87	8.96
State 8	46.90	−0.71	1.50	8.77	9.31	9.39
State 9	49.00	−0.78	0.40	8.23	8.66	8.74

Three data samples of an average of 10 s each were recorded for every axis and every different operation state. On the z axis, the gravity acceleration is included in the measured values. The same sampling methodology was followed for obtaining sound data.

2.3. Data Processing

The used datasets were all trimmed to a length of 5000 ms for each sample, and the transformation from time to frequency domain was applied using a Fast Fourier Transform on the recorded signals. The MATLAB® `fft()` function was used for the transform.

Cavitation-induced instabilities produce distinct frequency components that can be identified and further analyzed. As shown in Figure 5b, one of the main characteristics of both vibration and sound signals that was analyzed is the amplitude at specific frequencies. The pre-processing of the data was limited, aiming to exclude inputs during the first and last seconds of the sampling period, where it is most possible that the operator of the instruments affected the sampling process (either by mounting the instruments in place or hitting the record button). Only the operator-induced noise was removed by this processing method, since in a real-time application, the operator will not interfere during data acquisition. By applying minimum processing to the acquired data, classification methods were assessed for dealing with unavoidable signal noise (e.g., water flow-induced vibration). In addition, identifying the simplest algorithm using minimum computational time and power was attempted for future implementation of a real-time, low-cost, yet reliable application for smartphones capable of alarming the operator for evolving cavitation. In that sense, no features/characteristics extraction method was implemented, and raw data (after FFT transformation) were used directly.

Two samples from each state were used for training each classification algorithm, and one sample was used for testing. For the CNN, samples of 5 s and 2500 points were used to create the corresponding spectrograms for training and testing.

Data were plotted in the time domain to perform a preliminary comparison by visually inspecting the produced graphs of the different states in comparison with the reference state. Analysis in the time domain allows for the detection of transient events, such as the intermittent occurrence of cavitation bubbles collapsing. In addition, datasets were transformed into spectrograms using the `spectrogram()` function of MATLAB[®]. The produced images were visually inspected, and limited differentiation among different states could be observed only on the frequency domain plots. Figure 5 shows the produced plots and spectrograms directly from MATLAB[®], only for State 2 (the best efficiency operating state of the pump), for informational purposes only, as it is impossible to draw useful conclusions by mere visual observation.

It is worth noting that more complicated analysis techniques, like envelope analysis, were not employed in this research due to their complexity and higher processing times, which would make the classification of signals in real-time more difficult and would require higher computational capacity. Furthermore, techniques as such apply in more delicate systems where external factors are not affecting the obtained signal as much as in a lifelike industrial irrigation system.

Four different classification methods were utilized to classify the datasets. These methods were implemented using MATLAB[®] libraries and corresponding algorithms.

The first method employed was the classification tree, or decision tree theory. In MATLAB[®], the classification algorithm is based on the C4.5 algorithm, which constructs decision trees using information entropy. The algorithm recursively splits the dataset based on input values to minimize entropy and maximize information gain [25]. The decision tree predicts the class or value of the response variable by learning the decision rule from the training dataset. Starting at the root node, it predicts the class label using the decision tree. The internal node splits based on the properties of the root node, while the leaf node, located at the bottom of the internal node, contains the predicted value of the class label or response variable and does not split further. The decision tree is highly interpretable, requiring no statistical knowledge, and does not assume a specific data type. It is robust to multi-collinearity and outliers [26].

The second method is based on KNN classification. The k-Nearest Neighbors (k-NN) algorithm is a simple and effective classification method in machine learning and pattern recognition. It is a non-parametric approach that predicts based on the similarity of input features to labeled samples in the training dataset [27]. To classify a data record, its k nearest neighbors are retrieved, forming a neighborhood. Majority voting among the data records in the neighborhood is typically used to determine the classification of the data record, with or without distance-based weighting [28].

The third method employed support vector machines (SVMs), which are supervised learning models used for information analysis and pattern recognition. SVM is a powerful algorithm for classification and regression tasks, particularly suited for high-dimensional data. It can handle both linear and non-linear decision boundaries. The main concept behind SVM classification is to find an optimal hyperplane that maximally separates the classes in the feature space. The chosen hyperplane has the largest margin, which represents the perpendicular distance between the hyperplane and the closest data points from each class, known as support vectors [29]. SVM is used for both classification and regression tasks, with a training stage to build a classifier. The SVM training algorithm constructs a model that assigns new samples to specific categories, making it a non-probabilistic binary linear classifier [30].

Lastly, a CNN classification method was implemented using spectrograms created from the data. Convolutional neural networks (CNNs) are deep learning architectures that are highly effective for image classification. CNNs automatically learn and extract hierarchical patterns and features from input images, resulting in highly accurate classification outcomes [31]. CNNs consist of convolutional layers, pooling layers, and fully connected layers. Feature extraction and classification for 2D images are performed within a single network architecture. CNNs excel at learning and optimizing filters during the training step, surpassing the time-consuming manual feature engineering typically required for complex data. Additionally, CNNs do not rely on prior expert knowledge [32].

The hyperparameter optimization process was automated in all the methods by utilizing the automatic method provided in MATLAB[®]. This approach allowed the algorithms to automatically search for the best set of hyperparameters based on the specified search method and performance metric. The algorithms explored different combinations of hyperparameters, automatically adjusting their values to find the optimal configuration for the given datasets.

During the training process, the algorithms iteratively evaluated different hyperparameter settings and assessed their impact on the model's performance using the chosen performance metric. This automated search allowed for efficient exploration of the hyperparameter space, ultimately leading to improved models with optimized hyperparameters.

3. Results and Discussion

The results of the four different methods used for the classification of vibration and sound data are presented in this section. For the vibration signals, each method was applied to the data taken from all three axes of the three-dimensional coordinate system. Sound signal analysis results are presented in the first part of this section.

3.1. Sound Signal Analysis Results

Figure 6 displays the results obtained from the analysis of sound signals using the four classification methods: classification tree (shown in orange), KNN (shown in red), SVM (shown in blue), and CNN (shown in green). The success rates of classification for each of the ten states are represented by the colored bars. It is important to note that each classification method has its own strengths and weaknesses when classifying specific states. However, there are certain patterns observed in the success or failure of the classification methods.

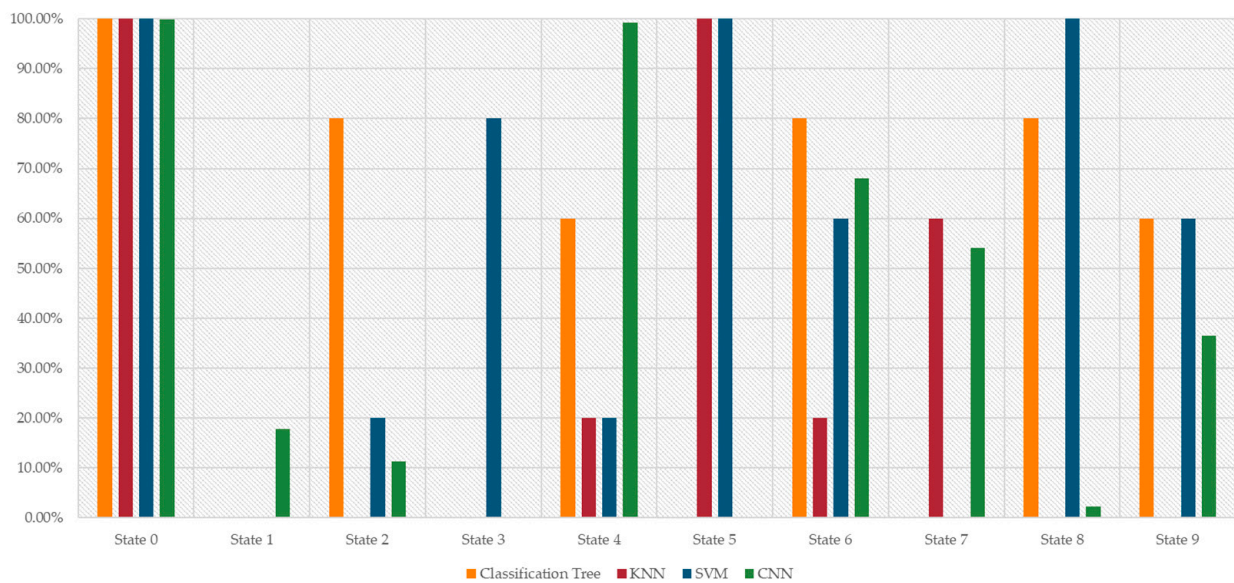


Figure 6. Success Rate (%) of different methods for sound data for Classification Tree method, KNN method, SVM method and CNN method.

For example, State 0 achieved a 100.00% success rate across all three methods, while State 1 had a 0.00% success rate. There are also similarities in the performance of the methods in other states. The SVM method appears to be the most successful, as its accuracy surpasses that of the classification tree and KNN methods. Although the KNN method identified the fewest number of states, it stands out by successfully identifying State 7 with a 60.00% success rate.

In comparison, the CNN method is almost 100.00% successful for classifying States 0 and 4 and adequately successful for State 6, with 67.99% of the data correctly classified. It has a 0.00% success rate for States 3 and 5 and a close to zero success rate for State 8. As will be discussed further in Section 3, the success rate of the CNN method for the sound data is between the success rates of the classification tree and the KNN method.

These results highlight that there is no optimal method for identifying and classifying all situations. Each method has its own strengths and limitations, and its effectiveness varies depending on the specific method being classified.

Figure 7 shows the classification for the four methods in a confusion matrix. The confusion matrix is a very popular measure used while solving classification problems. It is a square matrix summarizing the predicted and actual classifications for each class. Each cell represents the number of instances from the actual class i that were predicted as class j . The cells in the main diagonal represent the true positive (TP) values, indicating the instances that were correctly classified for each class. The off-diagonal cells represent the false positive (FP) values, indicating instances that were incorrectly classified as class j instead of class i . The different colors in Figure 7 subfigures are used for consistency with the four different colors used in Figure 6.

Classification Tree

		Predicted Class									
		State 0	State 1	State 2	State 3	State 4	State 5	State 6	State 7	State 8	State 9
Actual Class	State 0	5 100.00%	0 0.00%	0 0.00%	0 0.00%	0 0.00%	0 0.00%	0 0.00%	0 0.00%	0 0.00%	0 0.00%
	State 1	0 0.00%	0 0.00%	1 20.00%	0 0.00%	1 20.00%	0 0.00%	0 0.00%	0 0.00%	3 60.00%	0 0.00%
	State 2	0 0.00%	0 0.00%	4 80.00%	0 0.00%	0 0.00%	0 0.00%	1 20.00%	0 0.00%	0 0.00%	0 0.00%
	State 3	0 0.00%	0 0.00%	4 80.00%	0 0.00%	0 0.00%	0 0.00%	0 0.00%	0 0.00%	1 20.00%	0 0.00%
	State 4	0 0.00%	1 20.00%	0 0.00%	0 0.00%	3 60.00%	0 0.00%	1 20.00%	0 0.00%	0 0.00%	0 0.00%
	State 5	0 0.00%	0 0.00%	0 0.00%	0 0.00%	3 60.00%	0 0.00%	2 40.00%	0 0.00%	0 0.00%	0 0.00%
	State 6	0 0.00%	0 0.00%	0 0.00%	0 0.00%	0 0.00%	0 0.00%	4 80.00%	0 0.00%	1 20.00%	0 0.00%
	State 7	0 0.00%	1 20.00%	0 0.00%	0 0.00%	0 0.00%	0 0.00%	0 0.00%	0 0.00%	4 80.00%	0 0.00%
	State 8	0 0.00%	0 0.00%	0 0.00%	0 0.00%	0 0.00%	0 0.00%	1 20.00%	0 0.00%	4 80.00%	0 0.00%
	State 9	1 20.00%	0 0.00%	0 0.00%	0 0.00%	0 0.00%	0 0.00%	0 0.00%	0 0.00%	1 20.00%	3 60.00%

(a)

KNN

		Predicted Class									
		State 0	State 1	State 2	State 3	State 4	State 5	State 6	State 7	State 8	State 9
Actual Class	State 0	5 100.00%	0 0.00%	0 0.00%	0 0.00%	0 0.00%	0 0.00%	0 0.00%	0 0.00%	0 0.00%	0 0.00%
	State 1	0 0.00%	0 0.00%	5 100.00%	0 0.00%	0 0.00%	0 0.00%	0 0.00%	0 0.00%	0 0.00%	0 0.00%
	State 2	0 0.00%	0 0.00%	0 0.00%	5 100.00%	0 0.00%	0 0.00%	0 0.00%	0 0.00%	0 0.00%	0 0.00%
	State 3	0 0.00%	0 0.00%	0 0.00%	0 0.00%	5 100.00%	0 0.00%	0 0.00%	0 0.00%	0 0.00%	0 0.00%
	State 4	0 0.00%	0 0.00%	0 0.00%	0 0.00%	1 20.00%	0 0.00%	4 80.00%	0 0.00%	0 0.00%	0 0.00%
	State 5	0 0.00%	0 0.00%	0 0.00%	0 0.00%	0 0.00%	5 100.00%	0 0.00%	0 0.00%	0 0.00%	0 0.00%
	State 6	0 0.00%	0 0.00%	0 0.00%	0 0.00%	0 0.00%	0 0.00%	1 20.00%	4 80.00%	0 0.00%	0 0.00%
	State 7	0 0.00%	0 0.00%	0 0.00%	0 0.00%	0 0.00%	0 0.00%	0 0.00%	3 60.00%	2 40.00%	0 0.00%
	State 8	0 0.00%	0 0.00%	0 0.00%	0 0.00%	0 0.00%	0 0.00%	0 0.00%	0 0.00%	0 0.00%	5 100.00%
	State 9	0 0.00%	0 0.00%	0 0.00%	0 0.00%	0 0.00%	5 100.00%	0 0.00%	0 0.00%	0 0.00%	0 0.00%

(b)

SVM

		Predicted Class									
		State 0	State 1	State 2	State 3	State 4	State 5	State 6	State 7	State 8	State 9
Actual Class	State 0	5 100.00%	0 0.00%	0 0.00%	0 0.00%	0 0.00%	0 0.00%	0 0.00%	0 0.00%	0 0.00%	0 0.00%
	State 1	0 0.00%	0 0.00%	5 100.00%	0 0.00%	0 0.00%	0 0.00%	0 0.00%	0 0.00%	0 0.00%	0 0.00%
	State 2	0 0.00%	0 0.00%	1 20.00%	4 80.00%	0 0.00%	0 0.00%	0 0.00%	0 0.00%	0 0.00%	0 0.00%
	State 3	0 0.00%	0 0.00%	0 0.00%	4 80.00%	1 20.00%	0 0.00%	0 0.00%	0 0.00%	0 0.00%	0 0.00%
	State 4	0 0.00%	0 0.00%	0 0.00%	0 0.00%	1 20.00%	0 0.00%	4 80.00%	0 0.00%	0 0.00%	0 0.00%
	State 5	0 0.00%	0 0.00%	0 0.00%	0 0.00%	0 0.00%	5 100.00%	0 0.00%	0 0.00%	0 0.00%	0 0.00%
	State 6	0 0.00%	0 0.00%	0 0.00%	0 0.00%	0 0.00%	0 0.00%	3 60.00%	2 40.00%	0 0.00%	0 0.00%
	State 7	0 0.00%	0 0.00%	0 0.00%	0 0.00%	0 0.00%	0 0.00%	0 0.00%	0 0.00%	5 100.00%	0 0.00%
	State 8	0 0.00%	0 0.00%	0 0.00%	0 0.00%	0 0.00%	0 0.00%	0 0.00%	0 0.00%	5 100.00%	0 0.00%
	State 9	2 40.00%	0 0.00%	0 0.00%	0 0.00%	0 0.00%	0 0.00%	0 0.00%	0 0.00%	0 0.00%	3 60.00%

(c)

Figure 7. Cont.

CNN

		Predicted Class									
		State 0	State 1	State 2	State 3	State 4	State 5	State 6	State 7	State 8	State 9
Actual Class	State 0	5 99.91%	0 0.09%	0 0.00%	0 0.00%	0 0.00%	0 0.00%	0 0.00%	0 0.00%	0 0.00%	0 0.00%
	State 1	0 0.00%	1 17.86%	1 16.48%	0 0.00%	0 0.00%	0 0.00%	3 65.66%	0 0.01%	0 0.00%	0 0.00%
	State 2	0 0.00%	0 0.86%	1 11.36%	0 0.00%	0 0.00%	0 0.00%	4 78.24%	0 9.25%	0 0.03%	0 0.26%
	State 3	0 0.00%	0 0.01%	0 4.68%	0 0.00%	5 93.78%	0 0.00%	0 0.00%	0 0.00%	0 0.00%	0 1.53%
	State 4	0 0.00%	0 0.00%	0 0.00%	0 0.00%	5 99.30%	0 0.00%	0 0.00%	0 0.00%	0 0.00%	0 0.70%
	State 5	0 0.00%	0 0.00%	0 0.00%	0 0.00%	0 0.00%	0 0.00%	5 100.00%	0 0.00%	0 0.00%	0 0.00%
	State 6	0 0.00%	0 0.17%	1 15.73%	0 0.00%	0 0.00%	0 0.00%	3 67.99%	1 16.11%	0 0.00%	0 0.01%
	State 7	0 0.00%	0 0.02%	0 0.09%	0 0.00%	0 0.00%	0 0.00%	1 27.00%	3 54.16%	0 0.15%	1 18.59%
	State 8	0 0.00%	0 0.00%	0 0.00%	0 0.00%	0 0.00%	0 0.00%	0 0.00%	0 0.49%	0 2.28%	5 97.23%
	State 9	0 0.00%	0 0.00%	0 0.00%	0 0.00%	3 63.41%	0 0.01%	0 0.00%	0 0.00%	0 0.00%	2 36.58%

(d)

Figure 7. Confusion Matrices for Sound Data (a) Classification Tree method (b) KNN method (c) SVM method (d) CNN method.

When using the Classification Tree method, as shown in Figure 7a, only the datasets for State 0 are 100.00% correctly classified, which was expected since it is the state that differs the most from the others. The highest success classification rate apart from State 0 is for States 2, 6, and 8, with 80.00% of the data correctly classified. The method is greatly unsuccessful in identifying State 1, which is wrongly classified as State 2 for 20.00% of the datasets, as State 4 for another 20% of the datasets, and as State 8 for 60.00% of the datasets. Additionally, although 60.00% of the data for State 9 is correctly classified, 20.00% of the data for State 9 is classified as State 0, and 20.00% of the data is classified as State 8.

Figure 7b demonstrates that by using the KNN method, States 0 and 5 are classified correctly at 100%, followed by 60.00% of the data classified correctly as State 7. For States 1, 2, 3, 8, and 9, the entirety of the datasets is falsely classified. Figure 7c shows the better accuracy of the SVM method compared to the other two, with 100.00% of the data correctly classified in States 0, 5, and 8. Additionally, 80% of the data for State 3 and 60.00% of the data for States 6 and 9 are successfully classified. However, for State 9, 20.00% of the data is classified as State 0, which differs a lot from State 9.

Figure 7d, the confusion matrix of the CNN method, shows that the method has successfully classified States 0 and 4 and classified with average accuracy States 6 and 7. What is worth noting is that the CNN method falsely classifies State 3 as State 4 and State 5 as State 6. Given these results and the overall accuracy of the classification, the CNN method is not deemed appropriate to classify sound data.

3.2. Vibration Signal Analysis Results

3.2.1. Classification Tree Method Results

Figure 8 presents the results of the classification tree method. Each shaded bar represents the success rate of the classification method for each axis and each of the ten states.

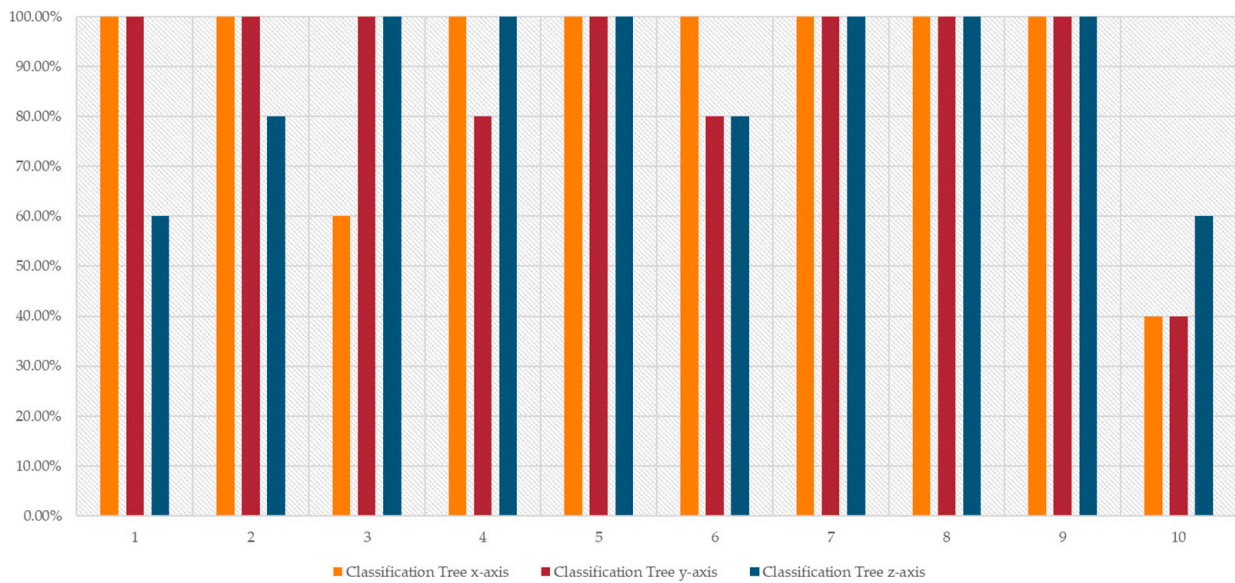


Figure 8. Success rate (%) of the classification tree method for all states and for all axes.

The figure reveals that most states and axes achieve a 100.00% success rate. However, for State 0 on the z-axis, the success rate drops to 60.00%. States 1, 3, and 5 show an 80.00% success rate on the z-axis, while States 3 and 5 exhibit an 80.00% success rate on the y-axis. State 2 has a 60.00% success rate on the x-axis, and State 4 achieves a 100.00% success rate on all axes. States 6 through 8 attain 100.00% accuracy in classification. In contrast, State 9 shows deviations on all axes, with less than half of the data correctly classified for the x- and y-axes, resulting in a 40.00% success rate and a 60.00% success rate for the z-axis.

What is of greater value, rather than just observing the success rate of the method, is the confusion matrix of each axis. Figure 9 shows the actual and predicted states for each axis for the Classification Tree method. Classes 0–9 correspond to States 0–9 as described in Table 2. Different colors in Figure 9 subfigures are used for consistency with the colors in Figure 8.

Classification Tree x-axis

		Predicted Class									
		State 0	State 1	State 2	State 3	State 4	State 5	State 6	State 7	State 8	State 9
Actual Class	State 0	5 100.00%	0 0.00%	0 0.00%	0 0.00%	0 0.00%	0 0.00%	0 0.00%	0 0.00%	0 0.00%	0 0.00%
	State 1	0 0.00%	5 100.00%	0 0.00%	0 0.00%	0 0.00%	0 0.00%	0 0.00%	0 0.00%	0 0.00%	0 0.00%
	State 2	0 0.00%	2 40.00%	3 60.00%	0 0.00%	0 0.00%	0 0.00%	0 0.00%	0 0.00%	0 0.00%	0 0.00%
	State 3	0 0.00%	0 0.00%	0 0.00%	5 100.00%	0 0.00%	0 0.00%	0 0.00%	0 0.00%	0 0.00%	0 0.00%
	State 4	0 0.00%	0 0.00%	0 0.00%	0 0.00%	5 100.00%	0 0.00%	0 0.00%	0 0.00%	0 0.00%	0 0.00%
	State 5	0 0.00%	0 0.00%	0 0.00%	0 0.00%	0 0.00%	5 100.00%	0 0.00%	0 0.00%	0 0.00%	0 0.00%
	State 6	0 0.00%	0 0.00%	0 0.00%	0 0.00%	0 0.00%	0 0.00%	5 100.00%	0 0.00%	0 0.00%	0 0.00%
	State 7	0 0.00%	0 0.00%	0 0.00%	0 0.00%	0 0.00%	0 0.00%	0 0.00%	5 100.00%	0 0.00%	0 0.00%
	State 8	0 0.00%	0 0.00%	0 0.00%	0 0.00%	0 0.00%	0 0.00%	0 0.00%	0 0.00%	5 100.00%	0 0.00%
	State 9	0 0.00%	0 0.00%	0 0.00%	0 0.00%	0 0.00%	0 0.00%	0 0.00%	0 0.00%	3 60.00%	2 40.00%

(a)

Figure 9. Cont.

Classification Tree y-axis

		Predicted Class									
		State 0	State 1	State 2	State 3	State 4	State 5	State 6	State 7	State 8	State 9
Actual Class	State 0	5 100.00%	0 0.00%	0 0.00%	0 0.00%	0 0.00%	0 0.00%	0 0.00%	0 0.00%	0 0.00%	0 0.00%
	State 1	0 0.00%	5 100.00%	0 0.00%	0 0.00%	0 0.00%	0 0.00%	0 0.00%	0 0.00%	0 0.00%	0 0.00%
	State 2	0 0.00%	0 0.00%	5 100.00%	0 0.00%	0 0.00%	0 0.00%	0 0.00%	0 0.00%	0 0.00%	0 0.00%
	State 3	0 0.00%	0 0.00%	0 0.00%	4 80.00%	1 20.00%	0 0.00%	0 0.00%	0 0.00%	0 0.00%	0 0.00%
	State 4	0 0.00%	0 0.00%	0 0.00%	0 0.00%	5 100.00%	0 0.00%	0 0.00%	0 0.00%	0 0.00%	0 0.00%
	State 5	1 20.00%	0 0.00%	0 0.00%	0 0.00%	0 0.00%	4 80.00%	0 0.00%	0 0.00%	0 0.00%	0 0.00%
	State 6	0 0.00%	0 0.00%	0 0.00%	0 0.00%	0 0.00%	0 0.00%	5 100.00%	0 0.00%	0 0.00%	0 0.00%
	State 7	0 0.00%	0 0.00%	0 0.00%	0 0.00%	0 0.00%	0 0.00%	0 0.00%	5 100.00%	0 0.00%	0 0.00%
	State 8	0 0.00%	0 0.00%	0 0.00%	0 0.00%	0 0.00%	0 0.00%	0 0.00%	0 0.00%	5 100.00%	0 0.00%
	State 9	0 0.00%	0 0.00%	0 0.00%	0 0.00%	0 0.00%	0 0.00%	0 0.00%	1 20.00%	2 40.00%	2 40.00%

(b)

Classification Tree z-axis

		Predicted Class									
		State 0	State 1	State 2	State 3	State 4	State 5	State 6	State 7	State 8	State 9
Actual Class	State 0	3 60.00%	2 40.00%	0 0.00%	0 0.00%	0 0.00%	0 0.00%	0 0.00%	0 0.00%	0 0.00%	0 0.00%
	State 1	0 0.00%	4 80.00%	1 20.00%	0 0.00%	0 0.00%	0 0.00%	0 0.00%	0 0.00%	0 0.00%	0 0.00%
	State 2	0 0.00%	0 0.00%	5 100.00%	0 0.00%	0 0.00%	0 0.00%	0 0.00%	0 0.00%	0 0.00%	0 0.00%
	State 3	0 0.00%	0 0.00%	0 0.00%	5 100.00%	0 0.00%	0 0.00%	0 0.00%	0 0.00%	0 0.00%	0 0.00%
	State 4	0 0.00%	0 0.00%	0 0.00%	0 0.00%	5 100.00%	0 0.00%	0 0.00%	0 0.00%	0 0.00%	0 0.00%
	State 5	1 20.00%	0 0.00%	0 0.00%	0 0.00%	0 0.00%	4 80.00%	0 0.00%	0 0.00%	0 0.00%	0 0.00%
	State 6	0 0.00%	0 0.00%	0 0.00%	0 0.00%	0 0.00%	0 0.00%	5 100.00%	0 0.00%	0 0.00%	0 0.00%
	State 7	0 0.00%	0 0.00%	0 0.00%	0 0.00%	0 0.00%	0 0.00%	0 0.00%	5 100.00%	0 0.00%	0 0.00%
	State 8	0 0.00%	0 0.00%	0 0.00%	0 0.00%	0 0.00%	0 0.00%	0 0.00%	0 0.00%	5 100.00%	0 0.00%
	State 9	0 0.00%	0 0.00%	0 0.00%	0 0.00%	0 0.00%	0 0.00%	2 40.00%	0 0.00%	0 0.00%	3 60.00%

(c)

Figure 9. (a) Classification Tree confusion matrix for *x*-axis (b) Classification Tree confusion matrix for *y*-axis (c) Classification Tree confusion matrix for *z*-axis.

For the *x*-axis, 40.00% of the data are classified in State 2 rather than in their correct State 3. Similarly, 60.00% of the data is wrongly classified in State 8 rather than in State 9. For the *y*-axis, where the overall success rate is lower, 60.00% of the data are classified in State 0 instead of State 1. 20.00% of the data are classified in State 2 instead of State 1, 20.00% of the data are classified in State 0 instead of State 5, and finally, 40.00% of the data are classified in State 2 instead of State 9. The *z*-axis confusion matrix shows similar behavior to the *y*-axis. 80.00% of the data for State 3 is classified correctly, with the balance being classified as State 4. 20% of the data for State 5 is classified as State 0. Finally, part of the State 9 data is classified as State 7 (20.00%) and State 8 (40.00%).

3.2.2. K-Nearest Neighbors (KNN) Method Results

When compared to the classification tree method, the KNN method shows a great improvement in the classification success rate for all axes. Figure 10 shows the success rate in the form of a shaded bar chart for the three axes.

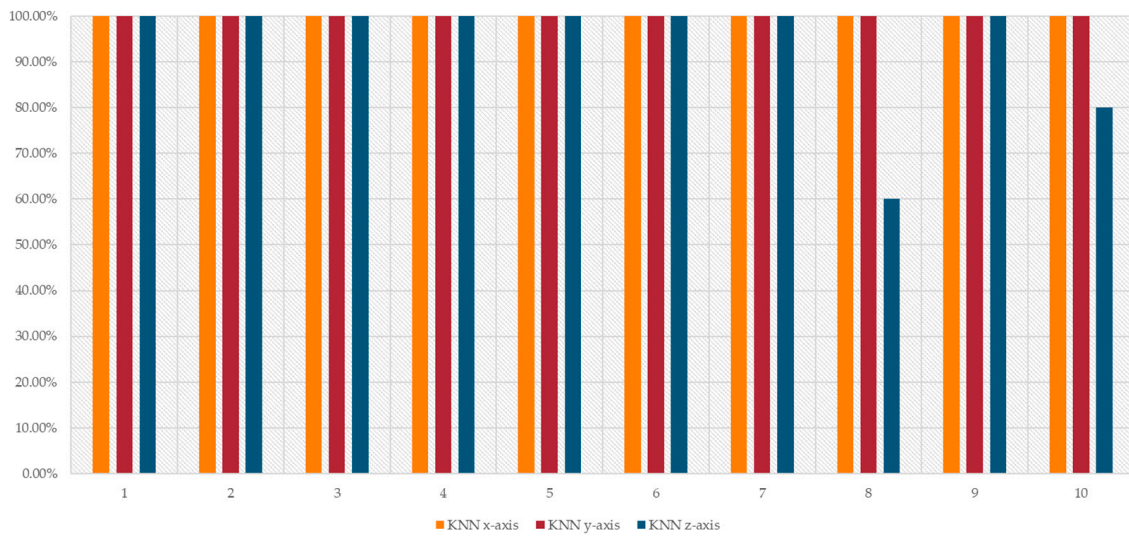


Figure 10. Success rate (%) of the KNN method for all states and for all axes.

The datasets that are not 100.00% classified correctly belong to States 7 and 9. For State 7, the KNN method fails to correctly classify 40.00% of the data on the z-axis, while this percentage drops to 20.00% for State 9 on the same axis.

Figure 11 shows the confusion matrices for the KNN method for all three axes. Classes 0–9 correspond to States 0–9 as described in Table 2. Different colors in Figure 11 subfigures are used for consistency with the colors in Figure 10.

KNN x-axis

		Predicted Class									
		State 0	State 1	State 2	State 3	State 4	State 5	State 6	State 7	State 8	State 9
Actual Class	State 0	5 100.00%	0 0.00%								
	State 1	0 0.00%	5 100.00%	0 0.00%							
	State 2	0 0.00%	0 0.00%	5 100.00%	0 0.00%						
	State 3	0 0.00%	0 0.00%	0 0.00%	5 100.00%	0 0.00%	0 0.00%	0 0.00%	0 0.00%	0 0.00%	0 0.00%
	State 4	0 0.00%	0 0.00%	0 0.00%	0 0.00%	5 100.00%	0 0.00%	0 0.00%	0 0.00%	0 0.00%	0 0.00%
	State 5	0 0.00%	0 0.00%	0 0.00%	0 0.00%	0 0.00%	5 100.00%	0 0.00%	0 0.00%	0 0.00%	0 0.00%
	State 6	0 0.00%	0 0.00%	0 0.00%	0 0.00%	0 0.00%	0 0.00%	5 100.00%	0 0.00%	0 0.00%	0 0.00%
	State 7	0 0.00%	0 0.00%	0 0.00%	0 0.00%	0 0.00%	0 0.00%	0 0.00%	5 100.00%	0 0.00%	0 0.00%
	State 8	0 0.00%	0 0.00%	0 0.00%	0 0.00%	0 0.00%	0 0.00%	0 0.00%	0 0.00%	5 100.00%	0 0.00%
	State 9	0 0.00%	0 0.00%	0 0.00%	0 0.00%	0 0.00%	0 0.00%	0 0.00%	0 0.00%	0 0.00%	5 100.00%

(a)

Figure 11. Cont.

KNN y-axis

		Predicted Class									
		State 0	State 1	State 2	State 3	State 4	State 5	State 6	State 7	State 8	State 9
Actual Class	State 0	5 100.00%	0 0.00%								
	State 1	0 0.00%	5 100.00%	0 0.00%							
	State 2	0 0.00%	0 0.00%	5 100.00%	0 0.00%						
	State 3	0 0.00%	0 0.00%	0 0.00%	5 100.00%	0 0.00%	0 0.00%	0 0.00%	0 0.00%	0 0.00%	0 0.00%
	State 4	0 0.00%	0 0.00%	0 0.00%	0 0.00%	5 100.00%	0 0.00%	0 0.00%	0 0.00%	0 0.00%	0 0.00%
	State 5	0 0.00%	0 0.00%	0 0.00%	0 0.00%	0 0.00%	5 100.00%	0 0.00%	0 0.00%	0 0.00%	0 0.00%
	State 6	0 0.00%	0 0.00%	0 0.00%	0 0.00%	0 0.00%	0 0.00%	5 100.00%	0 0.00%	0 0.00%	0 0.00%
	State 7	0 0.00%	0 0.00%	0 0.00%	0 0.00%	0 0.00%	0 0.00%	0 0.00%	5 100.00%	0 0.00%	0 0.00%
	State 8	0 0.00%	0 0.00%	0 0.00%	0 0.00%	0 0.00%	0 0.00%	0 0.00%	0 0.00%	5 100.00%	0 0.00%
	State 9	0 0.00%	0 0.00%	0 0.00%	0 0.00%	0 0.00%	0 0.00%	0 0.00%	0 0.00%	0 0.00%	5 100.00%

(b)

KNN z-axis

		Predicted Class									
		State 0	State 1	State 2	State 3	State 4	State 5	State 6	State 7	State 8	State 9
Actual Class	State 0	5 100.00%	0 0.00%	0 0.00%	0 0.00%	0 0.00%	0 0.00%	0 0.00%	0 0.00%	0 0.00%	0 0.00%
	State 1	0 0.00%	5 100.00%	0 0.00%	0 0.00%	0 0.00%	0 0.00%	0 0.00%	0 0.00%	0 0.00%	0 0.00%
	State 2	0 0.00%	0 0.00%	5 100.00%	0 0.00%	0 0.00%	0 0.00%	0 0.00%	0 0.00%	0 0.00%	0 0.00%
	State 3	0 0.00%	0 0.00%	0 0.00%	5 100.00%	0 0.00%	0 0.00%	0 0.00%	0 0.00%	0 0.00%	0 0.00%
	State 4	0 0.00%	0 0.00%	0 0.00%	0 0.00%	5 100.00%	0 0.00%	0 0.00%	0 0.00%	0 0.00%	0 0.00%
	State 5	0 0.00%	0 0.00%	0 0.00%	0 0.00%	0 0.00%	5 100.00%	0 0.00%	0 0.00%	0 0.00%	0 0.00%
	State 6	0 0.00%	0 0.00%	0 0.00%	0 0.00%	0 0.00%	0 0.00%	5 100.00%	0 0.00%	0 0.00%	0 0.00%
	State 7	0 0.00%	0 0.00%	0 0.00%	0 0.00%	0 0.00%	0 0.00%	2 40.00%	3 60.00%	0 0.00%	0 0.00%
	State 8	0 0.00%	0 0.00%	0 0.00%	0 0.00%	0 0.00%	0 0.00%	0 0.00%	0 0.00%	5 100.00%	0 0.00%
	State 9	0 0.00%	0 0.00%	0 0.00%	0 0.00%	0 0.00%	0 0.00%	0 0.00%	0 0.00%	1 20.00%	4 80.00%

(c)

Figure 11. (a) KNN confusion matrix for x-axis (b) KNN confusion matrix for y-axis (c) KNN confusion matrix for z-axis.

In total, 40.00% of the data that is wrongly classified as State 7 is classified as State 6. 20.00% of State 9 data is classified in State 8.

3.2.3. Support Vector Machines (SVM) Method Results

The SVM method produced similar results to the KNN method, with the classification success rate being significantly higher than that of its classification tree counterpart. As shown in Figure 12, nearly all datasets are classified in their corresponding states, with States 4 and 7 being exceptions. For those states, the algorithm successfully classified 80.00% of the data correctly on the z-axis.

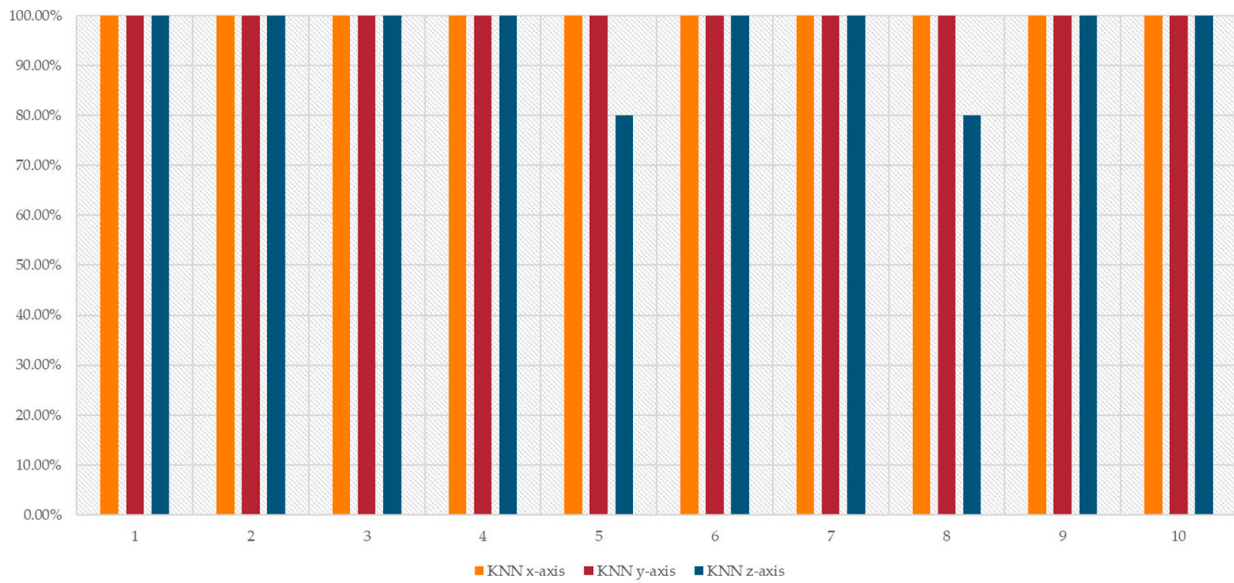


Figure 12. Success rate (%) of the SVM method for all states and for all axes.

Figure 13c shows the deviation in success rate for the z-axis discussed above. In more detail, 20.00% of the data in State 4 is classified in State 3, while 20.00% of the data in State 7 is classified in State 6. Different colors in Figure 13 subfigures are used for consistency with the colors in Figure 12.

SVM x-axis

		Predicted Class									
		State 0	State 1	State 2	State 3	State 4	State 5	State 6	State 7	State 8	State 9
Actual Class	State 0	5 100.00%	0 0.00%								
	State 1	0 0.00%	5 100.00%	0 0.00%							
	State 2	0 0.00%	0 0.00%	5 100.00%	0 0.00%						
	State 3	0 0.00%	0 0.00%	0 0.00%	5 100.00%	0 0.00%	0 0.00%	0 0.00%	0 0.00%	0 0.00%	0 0.00%
	State 4	0 0.00%	0 0.00%	0 0.00%	0 0.00%	5 100.00%	0 0.00%	0 0.00%	0 0.00%	0 0.00%	0 0.00%
	State 5	0 0.00%	0 0.00%	0 0.00%	0 0.00%	0 0.00%	5 100.00%	0 0.00%	0 0.00%	0 0.00%	0 0.00%
	State 6	0 0.00%	0 0.00%	0 0.00%	0 0.00%	0 0.00%	0 0.00%	5 100.00%	0 0.00%	0 0.00%	0 0.00%
	State 7	0 0.00%	0 0.00%	0 0.00%	0 0.00%	0 0.00%	0 0.00%	0 0.00%	5 100.00%	0 0.00%	0 0.00%
	State 8	0 0.00%	0 0.00%	0 0.00%	0 0.00%	0 0.00%	0 0.00%	0 0.00%	0 0.00%	5 100.00%	0 0.00%
	State 9	0 0.00%	0 0.00%	0 0.00%	0 0.00%	0 0.00%	0 0.00%	0 0.00%	0 0.00%	0 0.00%	5 100.00%

(a)

Figure 13. Cont.

SVM y-axis

		Predicted Class									
		State 0	State 1	State 2	State 3	State 4	State 5	State 6	State 7	State 8	State 9
Actual Class	State 0	5 100.00%	0 0.00%								
	State 1	0 0.00%	5 100.00%	0 0.00%							
	State 2	0 0.00%	0 0.00%	5 100.00%	0 0.00%						
	State 3	0 0.00%	0 0.00%	0 0.00%	5 100.00%	0 0.00%	0 0.00%	0 0.00%	0 0.00%	0 0.00%	0 0.00%
	State 4	0 0.00%	0 0.00%	0 0.00%	0 0.00%	5 100.00%	0 0.00%	0 0.00%	0 0.00%	0 0.00%	0 0.00%
	State 5	0 0.00%	0 0.00%	0 0.00%	0 0.00%	0 0.00%	5 100.00%	0 0.00%	0 0.00%	0 0.00%	0 0.00%
	State 6	0 0.00%	0 0.00%	0 0.00%	0 0.00%	0 0.00%	0 0.00%	5 100.00%	0 0.00%	0 0.00%	0 0.00%
	State 7	0 0.00%	0 0.00%	0 0.00%	0 0.00%	0 0.00%	0 0.00%	0 0.00%	5 100.00%	0 0.00%	0 0.00%
	State 8	0 0.00%	0 0.00%	0 0.00%	0 0.00%	0 0.00%	0 0.00%	0 0.00%	0 0.00%	5 100.00%	0 0.00%
	State 9	0 0.00%	0 0.00%	0 0.00%	0 0.00%	0 0.00%	0 0.00%	0 0.00%	0 0.00%	0 0.00%	5 100.00%

(b)

SVM z-axis

		Predicted Class									
		State 0	State 1	State 2	State 3	State 4	State 5	State 6	State 7	State 8	State 9
Actual Class	State 0	5 100.00%	0 0.00%	0 0.00%	0 0.00%	0 0.00%	0 0.00%	0 0.00%	0 0.00%	0 0.00%	0 0.00%
	State 1	0 0.00%	5 100.00%	0 0.00%	0 0.00%	0 0.00%	0 0.00%	0 0.00%	0 0.00%	0 0.00%	0 0.00%
	State 2	0 0.00%	0 0.00%	5 100.00%	0 0.00%	0 0.00%	0 0.00%	0 0.00%	0 0.00%	0 0.00%	0 0.00%
	State 3	0 0.00%	0 0.00%	0 0.00%	5 100.00%	0 0.00%	0 0.00%	0 0.00%	0 0.00%	0 0.00%	0 0.00%
	State 4	0 0.00%	0 0.00%	0 0.00%	1 20.00%	4 80.00%	0 0.00%	0 0.00%	0 0.00%	0 0.00%	0 0.00%
	State 5	0 0.00%	0 0.00%	0 0.00%	0 0.00%	0 0.00%	5 100.00%	0 0.00%	0 0.00%	0 0.00%	0 0.00%
	State 6	0 0.00%	0 0.00%	0 0.00%	0 0.00%	0 0.00%	0 0.00%	5 100.00%	0 0.00%	0 0.00%	0 0.00%
	State 7	0 0.00%	0 0.00%	0 0.00%	0 0.00%	0 0.00%	0 0.00%	1 20.00%	4 80.00%	0 0.00%	0 0.00%
	State 8	0 0.00%	0 0.00%	0 0.00%	0 0.00%	0 0.00%	0 0.00%	0 0.00%	0 0.00%	5 100.00%	0 0.00%
	State 9	0 0.00%	0 0.00%	0 0.00%	0 0.00%	0 0.00%	0 0.00%	0 0.00%	0 0.00%	0 0.00%	5 100.00%

(c)

Figure 13. (a) SVM confusion matrix for x-axis (b) SVM confusion matrix for y-axis (c) SVM confusion matrix for z-axis.

3.2.4. Convolutional Neural Network Results (CNN)

Comparison of the CNN classification results with the ones obtained from the three methods presented previously can provide a lead on which strategy is best to be followed when attempting to identify the operation conditions of a pump and, more specifically, the development of cavitation. Figure 14 shows the CNN classification success rate in the form of percentage bars for the different states and axes.

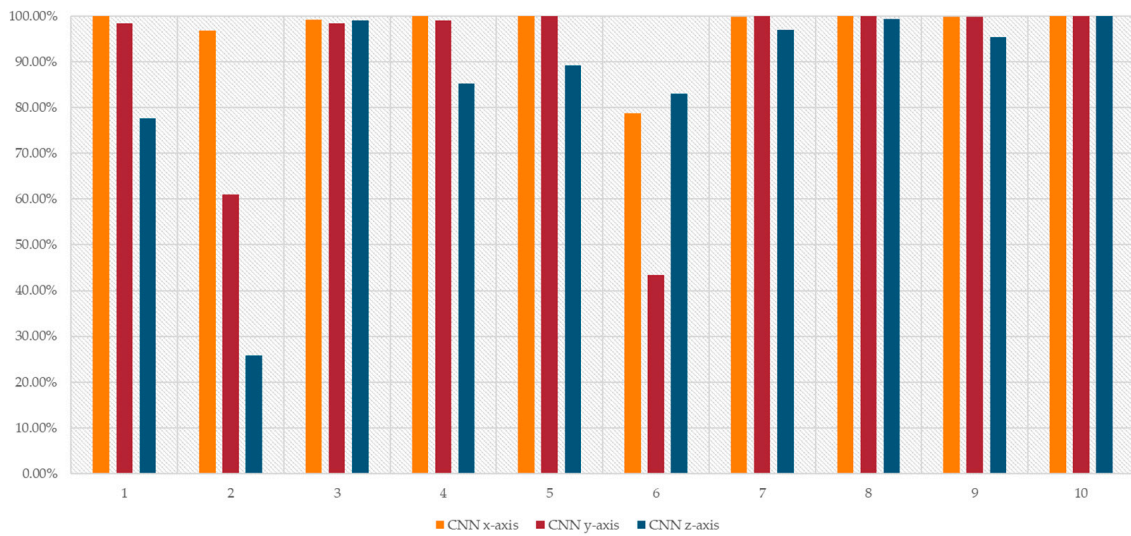


Figure 14. Success rate of the CNN method for all states and all axes.

The x-axis data showing major deviations in successful classification are the ones for State 5, where nearly 80.00% of the data are correctly classified. For the y-axis, nearly 60.00% of the data are classified correctly for State 1 and only 43.00% for State 5. Other states show almost 100.00% success rates in classification. The behavior for the z-axis is greatly different since it fails to identify State 1, which is the reference state, by achieving only a 25.80% success rate. Nearly 77.00% of the data is correctly classified for State 0. For states 2 to 5, the success rate ranges from nearly 83.00% to 99.00%. For the rest of the States, nearly all data is classified correctly. The above results are better depicted in Figure 15, the confusion matrix of the CNN method, which also shows the false positive values for the method. Different colors in Figure 15 subfigures are used for consistency with the colors in Figure 14.

CNN x-axis

		Predicted Class									
		State 0	State 1	State 2	State 3	State 4	State 5	State 6	State 7	State 8	State 9
Actual Class	State 0	5 99.97%	0 0.00%	0 0.00%	0 0.00%	0 0.00%	0 0.01%	0 0.01%	0 0.00%	0 0.01%	0 0.00%
	State 1	0 3.22%	5 96.78%	0 0.00%	0 0.00%	0 0.00%	0 0.00%	0 0.00%	0 0.00%	0 0.00%	0 0.00%
	State 2	0 0.12%	0 0.01%	5 99.27%	0 0.00%	0 0.00%	0 0.01%	0 0.60%	0 0.00%	0 0.01%	0 0.00%
	State 3	0 0.00%	0 0.00%	0 0.00%	5 100.00%	0 0.00%	0 0.00%	0 0.00%	0 0.00%	0 0.00%	0 0.00%
	State 4	0 0.00%	0 0.00%	0 0.00%	0 0.00%	5 100.00%	0 0.00%	0 0.00%	0 0.00%	0 0.00%	0 0.00%
	State 5	0 0.62%	0 0.00%	0 0.01%	0 0.00%	0 0.00%	4 78.73%	1 20.55%	0 0.00%	0 0.10%	0 0.00%
	State 6	0 0.01%	0 0.00%	0 0.00%	0 0.00%	0 0.00%	0 0.09%	5 99.89%	0 0.00%	0 0.00%	0 0.00%
	State 7	0 0.01%	0 0.00%	0 0.00%	0 0.00%	0 0.00%	0 0.00%	0 0.00%	5 99.98%	0 0.01%	0 0.00%
	State 8	0 0.09%	0 0.00%	0 0.00%	0 0.00%	0 0.00%	0 0.00%	0 0.03%	0 0.00%	5 99.88%	0 0.00%
	State 9	0 0.00%	0 0.00%	0 0.00%	0 0.01%	0 0.00%	0 0.00%	0 0.00%	0 0.00%	0 0.00%	5 99.99%

(a)

Figure 15. Cont.

CNN y-axis

		Predicted Class									
		State 0	State 1	State 2	State 3	State 4	State 5	State 6	State 7	State 8	State 9
Actual Class	State 0	5 98.33%	0 0.00%	0 0.79%	0 0.00%	0 0.00%	0 0.00%	0 0.07%	0 0.00%	0 0.80%	0 0.00%
	State 1	0 0.43%	3 61.05%	2 34.66%	0 0.17%	0 1.17%	0 0.00%	0 2.51%	0 0.01%	0 0.00%	0 0.00%
	State 2	0 1.49%	0 0.00%	5 98.47%	0 0.00%	0 0.00%	0 0.00%	0 0.00%	0 0.00%	0 0.03%	0 0.00%
	State 3	0 0.00%	0 0.00%	0 0.00%	5 98.98%	0 1.02%	0 0.00%	0 0.00%	0 0.00%	0 0.00%	0 0.00%
	State 4	0 0.00%	0 0.00%	0 0.00%	0 0.00%	5 100.00%	0 0.00%	0 0.00%	0 0.00%	0 0.00%	0 0.00%
	State 5	0 0.03%	0 0.00%	0 0.11%	0 0.03%	0 0.02%	2 43.46%	3 53.44%	0 2.75%	0 0.17%	0 0.00%
	State 6	0 0.00%	0 0.00%	0 0.00%	0 0.00%	0 0.00%	0 0.00%	5 100.00%	0 0.00%	0 0.00%	0 0.00%
	State 7	0 0.00%	0 0.00%	0 0.01%	0 0.00%	0 0.00%	0 0.00%	0 0.00%	5 99.98%	0 0.01%	0 0.00%
	State 8	0 0.00%	0 0.00%	0 0.00%	0 0.01%	0 0.01%	0 0.00%	0 0.01%	0 0.20%	5 99.78%	0 0.00%
	State 9	0 0.00%	0 0.00%	0 0.00%	0 0.00%	0 0.01%	0 0.00%	0 0.00%	0 0.00%	0 0.00%	5 99.98%

(b)

CNN z-axis

		Predicted Class									
		State 0	State 1	State 2	State 3	State 4	State 5	State 6	State 7	State 8	State 9
Actual Class	State 0	4 77.63%	0 3.95%	0 0.18%	0 0.45%	0 0.88%	0 3.25%	0 6.33%	0 0.51%	0 6.82%	0 0.00%
	State 1	0 0.12%	1 25.82%	2 39.41%	0 0.02%	0 0.02%	2 32.23%	0 1.42%	0 0.97%	0 0.00%	0 0.00%
	State 2	0 0.01%	0 0.04%	5 99.02%	0 0.39%	0 0.04%	0 0.00%	0 0.03%	0 0.36%	0 0.11%	0 0.00%
	State 3	0 0.00%	0 0.01%	1 14.26%	4 85.20%	0 0.08%	0 0.00%	0 0.00%	0 0.00%	0 0.44%	0 0.00%
	State 4	0 0.00%	0 0.00%	0 0.01%	1 10.59%	4 89.22%	0 0.00%	0 0.01%	0 0.01%	0 0.13%	0 0.04%
	State 5	0 0.00%	0 0.07%	0 0.16%	0 0.01%	0 0.00%	4 82.97%	1 16.76%	0 0.03%	0 0.00%	0 0.00%
	State 6	0 0.00%	0 1.69%	0 0.04%	0 0.01%	0 0.01%	0 1.00%	5 96.96%	0 0.27%	0 0.01%	0 0.01%
	State 7	0 0.00%	0 0.00%	0 0.18%	0 0.00%	0 0.01%	0 0.00%	0 0.05%	5 99.32%	0 0.43%	0 0.00%
	State 8	0 0.07%	0 0.00%	0 0.03%	0 0.34%	0 0.06%	0 0.00%	0 2.90%	0 1.20%	5 95.40%	0 0.00%
	State 9	0 0.00%	0 0.00%	0 0.00%	0 0.00%	0 0.00%	0 0.00%	0 0.00%	0 0.00%	0 0.00%	5 100.00%

(c)

Figure 15. (a) CNN confusion matrix for x-axis (b) CNN confusion matrix for y-axis (c) CNN confusion matrix for z-axis.

By further analyzing the vibration results of the CNN, one can observe that the accuracy of the method falls between the classification tree and the KNN method.

The discussed metrics for the four methods described above are presented in Table 5, and a summary of all key findings is shown in Table 6.

Table 5. Accuracy of the different classification methods for all three directional axes.

	C. Tree	KNN	SVM	CNN
Accuracy—sound	46.00%	30.00%	54.00%	38.94%
Accuracy—x	90.00%	100.00%	100.00%	97.45%
Accuracy—y	90.00%	100.00%	100.00%	90.00%
Accuracy—z	88.00%	94.00%	96.00%	85.15%

Table 6. Summarized key findings.

Method	Average Accuracy	Accuracy on x Axis	Comments
Sound Signals			
Classif. Tree	46.00%	-	Significant deviations for State 9. 0.00% success rate for States 1, 3, 5 and 7.
KNN	30.00%	-	0.00% success rate States 1, 2, 3, 8 and 9.
SVM	54.00%	-	Significant deviations for State 9. 0.00% success rate for States 1 and 7.
CNN	39.84%	-	Significant deviations for States 1, 2 and 8. 0.00% success rate for States 3 and 5.
Vibration signals			
Classif. Tree	89.33%	90%	Significant deviations for states 2 and 9 on the x -axis, Significant deviations for states 0, 1, 3, 5, and 9 on y and z axes
KNN	98.00%	100%	Significant deviations for states 7 and 9 on the z -axis
SVM	98.67%	100%	Deviations for states 4 and 7 on the z -axis
CNN	90.87%	97.45%	Deviations for state 5 on the x -axis Deviations (significant) for states 1 and 5 on the y -axis Significant deviations for state 1 and smaller deviations for states 0, 3, 4, and 5 on the z -axis

What is of great importance when interpreting the findings, as shown in Tables 5 and 6, is that the vibration pattern developed during the different operating conditions of the pump is dominant and more distinctive on the x -axis, either with fully closed suction or discharge valves or during different cavitation conditions developed, thus the success identification rate is higher compared to the other two axes. On the other hand, z -axis vibration signals were the least distinctive, due to the dumpers installed on the pump support base and the gravity affecting this axis.

Observing the accuracy results of the vibration data for the dominant x -axis, the most accurate classification methods are the KNN and the SVM, which achieved 100.00% success in identifying the pump's operating state. CNN achieves a 97.45% success rate, but due to the high computational power and data preparation requirements, it is considered inferior when used in this application. Finally, the classification tree algorithm achieves a lower success rate, concluding that this method can identify the cavitation phenomenon accurately only when it is fully developed. The accuracy of the results is significantly higher when using vibration data than sound data. Nevertheless, the SVM method is the most successful one for accurately classifying the datasets for sound data, with a success rate of 54.00%. As discussed previously and proven by other similar studies [33], sound data are not as reliable as vibration data since they are much more susceptible to ambient factors and environmental noises, greatly affecting the classification's success. This observation is validated when comparing the accuracy of the same method when classifying sound and vibration data. For all the methods examined in this research, the overall accuracy of vibration data classification is more than 50.00% higher than the accuracy of sound data classification, regardless of the method and algorithm employed.

4. Conclusions

The scope of this study was to assess the use of low-cost sensors in combination with well-proven machine-learning algorithms for the detection of cavitation phenomena and the normal operating conditions of centrifugal irrigation pumps. The simple but innovative approach of directly attaching the mobile phone device to the pump's casing and using the embedded data acquisition software proved to be more than enough to achieve our

goal. Advanced yet fast machine learning algorithms also proved to be more than adequate when applied to the correct signal datasets.

Digging deeper into the extracted results, it is observed that using a low-cost vibration sensor and classification algorithms, both suction and discharge cavitation phenomena can be identified with a great success rate. Not only the existence of cavitation is detected, but also the scale of the evolving phenomenon can be identified, in addition to the normal or extreme operating conditions of the pump.

Based on the findings of this work, a smartphone application can be developed using the embedded accelerometer sensor and data acquisition hardware and software. By using the data from only one axis (the x axis), applying minimum post-processing (sampling points grouping and FFT), and using a simple classification algorithm (KNN or SVM), the required computational resources will be minimal. The continuously increasing computing power of smartphones is more than enough to run the algorithms in real-time, and combined with smartphones' connectivity through Bluetooth, WiFi, and GSM technologies, such an application would be of great functionality and value for the agricultural machines' operators as a preventive maintenance tool.

Part of the scope of this study was also to investigate the success rate of the examined classification methods with sound data. Many studies have observed that the scale of the cavitation phenomenon is directly related to the frequency of the emitted sound from the setup. Sound datasets are easier to obtain compared to vibration datasets but require more complex preparation and handling to achieve similar success rates in classification since they are more sensitive to ambient noise and other external factors [8,34]. Sound data are unreliable on their own, mainly due to the influence of external sounds other than those directly relevant to the experimental data. Therewithal, this worsens in actual agricultural applications, where noise from the environment is potentially the most dominant parameter, causing faulty results during identifying states. As a result, the success rate for classifying the sound signals was very low.

Based on the results of this study, future work can focus on the most successful classification methods applied to x -axis vibration signals. Features/characteristics extraction methods can be tested and utilized, along with optimization of the classification methods in terms of training sets and specific calculation parameters. Pumps of different types, sizes, and setups can be assessed to evaluate the usability of the proposed method. In this experimental setup, an electric motor was driving the pump, but it would be very challenging to attempt to detect the operation state of a pump driven by a diesel engine, which produces severe noise in the form of sound and vibration itself. In addition, real-life conditions like noise and natural vibration sources, along with varying temperatures and densities of water, must be addressed and assessed. Finally, experiments and testing on real agricultural irrigation installations are underway, along with the commercialization of the most preferable method as an embedded application on a smartphone family of products.

Author Contributions: Conceptualization, M.K., X.E.P. and V.F.; methodology, M.K. and V.F.; software, M.K. and X.E.P.; validation, V.F.; writing—original draft preparation, M.K.; writing—review and editing, X.E.P., V.F. and D.P.; supervision, D.P. and V.F. All authors have read and agreed to the published version of the manuscript.

Funding: This research received no external funding.

Institutional Review Board Statement: Not applicable.

Informed Consent Statement: Not applicable.

Data Availability Statement: The data presented in this study are available upon request from the corresponding author.

Conflicts of Interest: The authors declare no conflict of interest.

References

1. Jelle, B. *World Agriculture: Towards 2015/2030; An FAO Perspective*; Food and Agriculture Organization of the United Nations: Rome, Italy, 2003.
2. Čdina, M. Detection of Cavitation Phenomenon in a Centrifugal Pump Using Audible Sound. *Mech. Syst. Signal Process.* **2003**, *17*, 1335–1347. [[CrossRef](#)]
3. Čdina, M.; Prezelj, J. Detection of Cavitation in Situ Operation of Kinetic Pumps: Effect of Cavitation on the Characteristic Discrete Frequency Component. *Appl. Acoust.* **2009**, *70*, 1175–1182. [[CrossRef](#)]
4. Shagluf, A.; Parkinson, S.; Longstaff, A.P.; Fletcher, S. Adaptive decision support for suggesting a machine tool maintenance strategy. *J. Qual. Maint. Eng.* **2018**, *24*, 376–399. [[CrossRef](#)]
5. Harihara, P.P.; Parlos, A.G. Sensorless Detection of Impeller Cracks in Motor Driven Centrifugal Pumps. *Des. Anal. Control Diagn. Fluid Power Syst.* **2008**, *5*, 17–23. [[CrossRef](#)]
6. Lei, Y.; Yang, B.; Jiang, X.; Jia, F.; Li, N.; Nandi, A.K. Applications of machine learning to machine fault diagnosis: A review roadmap. *Mech. Syst. Signal Process.* **2020**, *138*, 106587. [[CrossRef](#)]
7. Adefemi, A.; Ilesanmi, D.; Olusegun, O.; Chinoyelum, E.; Oluwole, A. An adaptive Industrial Internet of things (IIOT) base technology for prediction and control of cavitation in centrifugal pumps. *Procedia CIRP* **2020**, *91*, 927–934.
8. Mousmoulis, G.; Karlsen-Davies, N.; Aggidis, G.; Anagnostopoulos, I.; Papantonis, D. Experimental analysis of cavitation in a centrifugal pump using acoustic emission, vibration measurements and flow visualization. *Eur. J. Mech.-B/Fluids* **2019**, *75*, 300–311. [[CrossRef](#)]
9. Chen, X.; Huihui, Z.; Yijun, M. Analysis of vibration and noise induced by unsteady flow inside a centrifugal compressor. *Aerosp. Sci. Technol.* **2020**, *107*, 106286. [[CrossRef](#)]
10. Seyed, M.H.; Yihai, F.; Brandon, K.W. Predictive maintenance of pumps in civil infrastructure: State-of-the-art, challenges and future directions. *Autom. Constr.* **2022**, *134*, 104049. [[CrossRef](#)]
11. Yuxin, W.; Md Fashiar, R.; Honglun, X.; Tzu-Liang, B.T. Recent advances and trends of predictive maintenance from data-driven machine prognostics perspective. *Measurement* **2022**, *187*, 110276. [[CrossRef](#)]
12. Vishwakarma, M.; Purohit, R.; Harshlata, V.; Rajput, P. Vibration Analysis & Condition Monitoring for Rotating Machines: A Review. *Mater. Proc.* **2017**, *4*, 2659–2664. [[CrossRef](#)]
13. Neill, G.D.; Reuben, R.L.; Sandford, P.M.; Brown, E.R.; Steel, J.A. Detection of incipient cavitation in pumps using acoustic emission. *J. Process Mech. Eng.* **1997**, *211*, 267–277. [[CrossRef](#)]
14. Al Obaidi, A.R. Experimental Investigation of the Effect of Suction Valve Opening on the Performance and Detection of Cavitation in the Centrifugal Pump Based on Acoustic Analysis Technique. *Arch. Acoust.* **2019**, *44*, 59–69. [[CrossRef](#)]
15. Leighton, T.G.; Phelps, A.; Ramble, D.G.; Sharpe, D.A. Comparison of the abilities of eight acoustic techniques to detect and size a single bubble. *Ultrasonics* **1996**, *34*, 661–667. [[CrossRef](#)]
16. Kyparissis, S.D.; Margaris, D.P. Experimental Investigation and Passive Flow Control of a Cavitating Centrifugal Pump. *Int. J. Rotating Mach.* **2012**, *2012*, 248082. [[CrossRef](#)]
17. Wang, W.; Sun, H.; Guo, J.; Lao, L.; Wu, S.; Zhang, J. Experimental study on water pipeline leak using In-Pipe acoustic signal analysis and artificial neural network prediction. *Measurement* **2021**, *186*, 110094. [[CrossRef](#)]
18. Kumar, A.; Gandhi, C.P.; Zhou, Y.; Kumar, R.; Xiang, J. Improved deep convolution neural network (CNN) for the identification of defects in the centrifugal pump using acoustic images. *Appl. Acoust.* **2020**, *167*, 107399. [[CrossRef](#)]
19. Ling, B.; Ling, Z.; Xiaoping, J.; Qinglong, P.; Daoxing, Y. Vibration in a Multistage Centrifugal Pump under Varied Conditions. *Shock Vib.* **2019**, *2019*, 2057031. [[CrossRef](#)]
20. Hu, Q.; Ohata, E.F.; Silva, F.H.S.; Ramalho, L.B.G.; Han, T.; Reboucas Filho, P.P. A New Online Approach for Classification of Pumps Vibration Patterns based on Intelligent IoT system. *Measurement* **2019**, *151*, 107138. [[CrossRef](#)]
21. David, T.; Alexander, Y.; Robert, D. Pump Failure Detection Using Support Vector Data Descriptions. *Lect. Notes Comput. Sci.* **1999**, *1642*, 415–426. [[CrossRef](#)]
22. Abdelgayed, T.S.; Morsi, W.G.; Sidhu, T.S. Fault detection and classification based on co-training of semisupervised machine learning. *IEEE Trans. Ind. Electron.* **2017**, *65*, 1595–1605. [[CrossRef](#)]
23. Liu, J.; Yang, X. Learning to See the Vibration: A Neural Network for Vibration Frequency Prediction. *Sensors* **2018**, *18*, 2530. [[CrossRef](#)]
24. Cerneic, J.; Prezelj, J.; Cudina, M. Use of noise and vibration signal for detection and monitoring of cavitation in kinetic pumps. *J. Acoust. Soc. Am.* **2008**, *123*, 3316. [[CrossRef](#)]
25. Zhu, X.; Yan, H.; Wang, J.; Wu, S. Research and Application of the Improved Algorithm C4.5 on Decision Tree. In Proceedings of the IEEE 2009 International Conference on Test and Measurements (ICTM), Hong Kong, China, 5–6 December 2009; pp. 184–187. [[CrossRef](#)]
26. Kim, D.; Heo, T.-Y. Anomaly Detection with Feature Extraction Based on Machine Learning Using Hydraulic System IoT Sensor Data. *Sensors* **2022**, *22*, 2479. [[CrossRef](#)] [[PubMed](#)]
27. Moosavian, A.; Ahmadi, H.; Tabatabaefar, A.; Khazaei, M. Comparison of Two Classifiers; K-Nearest Neighbor and Artificial Neural Network, for Fault Diagnosis on a Main Engine Journal-Bearing. *Shock. Vib.* **2013**, *20*, 263–272. [[CrossRef](#)]

28. Gongde, G.; Hui, W.; David, B.; Yaxin, B.; Kieran, G. KNN Model-Based Approach in Classification. In *The Move to Meaningful Internet Systems 2003: CoopIS, DOA, and ODBASE. OTM 2003*; Lecture Notes in Computer Science; Springer: Berlin/Heidelberg, Germany, 2003; Volume 2888, pp. 986–996. [[CrossRef](#)]
29. Ashanira, M.D.; Azlan, M.Z.; Roselina, S. Overview of Support Vector Machine in Modeling Machine Performances. *Procedia Eng.* **2011**, *24*, 308–312. [[CrossRef](#)]
30. Asish, K.P.; Janani, S.R.; Rajiv, T. Prediction of flow blockages and impending cavitation in centrifugal pumps using Support Vector Machine (SVM) algorithms based on vibration measurements. *Measurement* **2018**, *130*, 44–56.
31. Luis, A.; Diego, A.; Carlos, A. Vibration analysis in bearing for failure prevention using CNN. *J. Braz. Soc. Mech. Sci. Eng.* **2020**, *42*, 628. [[CrossRef](#)]
32. Çınar, Z.M.; Abdussalam Nuhu, A.; Zeeshan, Q.; Korhan, O.; Asmael, M.; Safaei, B. Machine Learning in Predictive Maintenance towards Sustainable Smart Manufacturing in Industry 4.0. *Sustainability* **2020**, *12*, 8211. [[CrossRef](#)]
33. Kim, J.; Lee, H.; Jeong, S.; Ahn, S.H. Sound-based remote real-time multi-device operational monitoring system using a Convolutional Neural Network (CNN). *J. Manuf. Syst.* **2021**, *58A*, 431–441. [[CrossRef](#)]
34. Murovec, J.; Curovic, L.; Novakovic, T.; Prezelj, J. Psychoacoustic approach for cavitation detection in centrifugal pumps. *Appl. Acoust.* **2020**, *165*, 107323. [[CrossRef](#)]

Disclaimer/Publisher’s Note: The statements, opinions and data contained in all publications are solely those of the individual author(s) and contributor(s) and not of MDPI and/or the editor(s). MDPI and/or the editor(s) disclaim responsibility for any injury to people or property resulting from any ideas, methods, instructions or products referred to in the content.